Journal of Medicinal Chemistry

Article

pubs.acs.org/jmc

Development of a Novel Class of Mitochondrial Ubiquinol–Cytochrome *c* Reductase Binding Protein (UQCRB) Modulators as Promising Antiangiogenic Leads

Hye Jin Jung,[†,‡,∥] Misun Cho,[†,∥] Yonghyo Kim,[†] Gyoonhee Han,[†] and Ho Jeong Kwon*[,†,§]

[†]Department of Biotechnology, Translational Research Center for Protein Function Control, College of Life Science and Biotechnology, Yonsei University, Seoul 120-749, Republic of Korea

[‡]Department of Pharmaceutical Engineering, Sun Moon University, No. 100, Kalsan-ri, Tangjeong-myeon, Asan-si, Chungnam 336-708, Republic of Korea

[§]Department of Internal Medicine, College of Medicine, Yonsei University, Seoul 120-752, Republic of Korea

Supporting Information

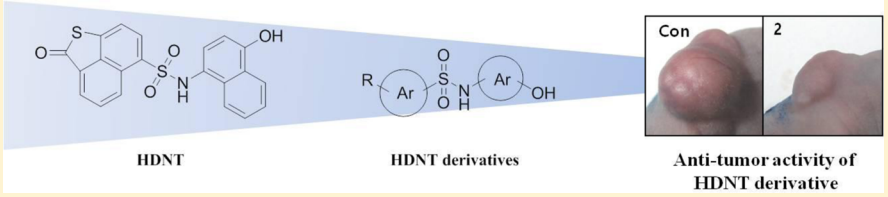

ABSTRACT: Recently, we identified a novel therapeutic target and a small molecule for regulating angiogenesis. Our study showed that ubiquinol–cytochrome *c* reductase binding protein (UQCRB) of the mitochondrial complex III plays a crucial role in hypoxia-induced angiogenesis via mitochondrial reactive oxygen species (ROS) mediated signaling. Herein, we developed new synthetic small molecules that specifically bind to UQCRB and regulate its function. To improve the pharmacological properties of 6-((1-hydroxynaphthalen-4-ylamino)dioxysulfone)-2*H*-naphtho[1,8-*bc*]thiophen-2-one (HDNT), a small molecule that targets UQCRB, a series of HDNT derivatives were designed and synthesized. Several derivatives showed a significant increase in hypoxia inducible factor 1α (HIF-1α) inhibitory potency compared to HDNT. The compounds bound to UQCRB and suppressed mitochondrial ROS-mediated hypoxic signaling, resulting in potent inhibition of angiogenesis without inducing cytotoxicity. Notably, one of these new derivatives significantly suppressed tumor growth in a mouse xenograft model. Therefore, these mitochondrial UQCRB modulators could be potential leads for the development of novel antiangiogenic agents.

INTRODUCTION

Angiogenesis, the formation of new blood vessels, is important in the pathogenesis of malignant, infectious, fibroproliferative, and inflammatory diseases.[1,2] In particular, tumor angiogenesis plays a crucial role in tumor propagation, tumor growth, and metastasis.[3−5] Therefore, the specific perturbation of angiogenesis has been considered a powerful strategy for the treatment of cancer and other angiogenesis-related human diseases. Several cellular target proteins that are important for angiogenesis and their specific inhibitors have been identified. However, recent clinical studies have revealed that the inhibition of these target proteins alone is not enough to block the complex biological processes involved in angiogenesis and tumor development.[6−12] Accordingly, the identification of novel therapeutic targets for angiogenesis regulation is helpful to reduce the rate of clinical failure and develop better antiangiogenic therapeutic agents.

Using a combination of phenotypic screening and the target identification method, we recently identified a new natural angiogenesis inhibitor terpestacin and its cognate target protein, ubiquinol–cytochrome *c* reductase binding protein (UQCRB) of mitochondrial complex III.[13,14] Our chemical genetics studies provided the first indication of UQCRB's role as a critical mediator of mitochondrial reactive oxygen species (ROS) mediated hypoxic signaling and the mode of action of terpestacin at the molecular and organism levels.[14,15] Accumulating evidence indicates that cellular oxygen sensing is required for hypoxia inducible factor (HIF) 1α stabilization, which is important for tumor cell survival, proliferation, and angiogenesis.[16,17] Under hypoxia, ROS generation at mitochondrial complex III inhibits the activity of prolyl hydroxylase enzymes (PHDs), thereby preventing HIF-1α proteasomal degradation and allowing its translocation to the nucleus and dimerization with HIF-1β, initiating the transcription of HIF-1 responsiveness genes.[18,19] We found that UQCRB is a crucial component of a mitochondrial O_2 sensor in complex III and thus regulates the generation of mitochondrial ROS, the key event in the signaling of cellular hypoxia.[14] Moreover, we demonstrated that terpestacin binding to UQCRB results in inhibition of hypoxia-induced ROS generation, and consequently, such inhibition blocks HIF activation and tumor

Received: June 7, 2014
Published: September 22, 2014

dx.doi.org/10.1021/jm500863j | *J. Med. Chem.* 2014, 57, 7990−7998

Scheme 1. General Procedure for the Synthesis of HDNT Derivatives[a]

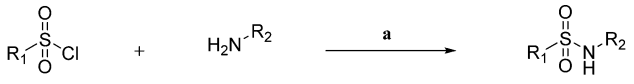

1

1a	R_1 = 4-Methylphenyl	R_2 = 4-Hydroxyphenyl
1b	R_1 = 4-Ethylphenyl	R_2 = 4-Hydroxyphenyl
1c	R_1 = 4-*t*-Butylphenyl	R_2 = 4-Hydroxyphenyl
1d	R_1 = 4-*t*-Butylphenyl	R_2 = 4-Hydroxynaphthalen-1-yl
1e	R_1 = 4-*t*-Butylphenyl	R_2 = 8-Hydroxyquinolin-5-yl
1f	R_1 = 4-Biphenyl	R_2 = 4-Hydroxyphenyl
1g	R_1 = 4-Biphenyl	R_2 = 3-Fluoro-4-hydroxyphenyl
1h	R_1 = 4-Biphenyl	R_2 = 3-Chloro-4-hydroxyphenyl
1i	R_1 = 4-Biphenyl	R_2 = 3-Carboxy-4-hydroxyphenyl
1j	R_1 = 4-Biphenyl	R_2 = 4-Hydroxynaphthalen-1-yl
1k	R_1 = 4-Biphenyl	R_2 = 5-Hydroxynaphthalen-1-yl
1l	R_1 = 4-Biphenyl	R_2 = 7-Hydroxynaphthalen-1-yl
1m	R_1 = 4-Biphenyl	R_2 = 8-Hydroxyquinolin-5-yl
1n	R_1 = 2-Naphthyl	R_2 = 4-Hydroxyphenyl
1o	R_1 = Quinolin-8-yl	R_2 = 4-Hydroxyphenyl
1p	R_1 = 4-*t*-Butylphenyl	R_2 = 2-Hydroxyphenyl
1q	R_1 = 4-*t*-Butylphenyl	R_2 = 3-Hydroxyphenyl

[a]Reagents and conditions: (a) pyridine, acetone, microwave reactor, 100 °C, 40 min.

angiogenesis in vivo.[14] In addition, recent research has demonstrated that UQCRB-mediated mitochondrial ROS play a central role in hypoxic signaling in tumor cells as well as vascular endothelial growth factor (VEGF) signaling in endothelial cells (ECs).[20] These results demonstrate that UQCRB could be a promising therapeutic target for antiangiogenic and antitumor drug development.

On the basis of a target-based screen with structural information on the binding mode of terpestacin and UQCRB, a novel synthetic small molecule targeting UQCRB, 6-((1-hydroxynaphthalen-4-ylamino)dioxysulfone)-2*H*-naphtho[1,8-*bc*]thiophen-2-one (HDNT), was successfully identified and exhibited potent antiangiogenic activity by modulating the oxygen-sensing function of UQCRB.[21] Thus, HDNT can serve as a new synthetic small molecule probe to explore the role of UQCRB in angiogenesis and as a potential lead compound for medical applications.

In the present study, we designed and synthesized a series of HDNT derivatives with a sulfonylamide backbone and their biological activities were evaluated both in vitro and in vivo to further develop novel antiangiogenic agents targeting UQCRB. On the basis of structure–activity relationship (SAR) studies of the derivatives, we identified a novel class of mitochondrial UQCRB modulators with enhanced pharmacological potential. In addition, a salt form of the most promising HDNT derivative was synthesized to increase its aqueous solubility, and its antiangiogenic and antitumor effects were demonstrated in a glioblastoma mouse xenograft model.

RESULTS AND DISCUSSION

Chemistry. The general procedure for the synthesis of HDNT derivatives is illustrated in Schemes 1 and 2. Sulfonamide-based HDNT derivatives were produced from commercially available sulfonyl chloride and amine. The sulfonamide derivatives **1a–q** were synthesized by reacting commercially available sulfonyl chloride with diverse amines in acetone in the presence of pyridine in a microwave reactor (Scheme 1). The potassium salt of **1f** was prepared in the presence of potassium hydroxide in ethanol to obtain **2** in high yields (Scheme 2).

Scheme 2. Preparation of 2[a]

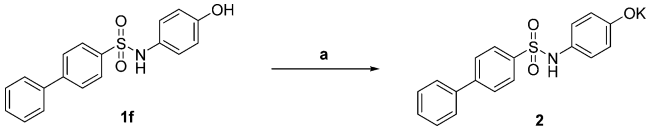

[a]Reagents and conditions: (a) KOH, EtOH, 0 °C.

SAR Study of HDNT Derivatives. Initially, HDNT derivatives were designed based on the docking study of HDNT and UQCRB. HDNT comprises the sulfonamide core and two major interacting parts with UQCRB: the 1-hydroxynaphthalene moiety for hydrogen bonding and hydrophobic interaction and the 2*H*-naphtho[1,8-*bc*]thiophen-2-one moiety for $\pi-\pi$ interaction with the active site of UQCRB.[21] To maintain the major interaction with UQCRB, HDNT derivatives have retained the sulfonamide core and introduced diverse functional groups to both sides of the sulfonamide core (Figure 1). All 17 HDNT derivatives were synthesized and biologically evaluated (Table 1). As the stability of HIF-1α represents a functional response to hypoxia triggered by the cellular oxygen sensing system, the bioactivity of the new synthetic compounds was evaluated by measuring HIF-1α protein levels using Western blot.[16,17] Various functional groups such as substituted phenyl (methyl, ethyl, *tert*-butyl, and biphenyl) and heterocycles (naphthyl and quinolinyl) were introduced on the R_1. Compounds containing small functional groups such as methyl and ethyl (**1a** and **1b**) showed lower HIF-1α inhibitory activities than compounds with the bulky functional groups such as *tert*-butyl and phenyl group (**1c** and **1f**). Especially **1f** with biphenyl group showed the best HIF-1α inhibitory activities (IC_{50} = 2.5 μM). The HDNT derivatives with heterocycles on R_1 showed no HIF-1α inhibitory activities (**1n** and **1o**). We introduced diverse functional groups including substituted phenyl, naphthyl, and quinolinyl on R_2. Hydroxy group was retained on R_2 for the hydrogen bonding interaction with UQCRB. **1f** with 4-hydroxyphenyl group on R_2 showed better HIF-1α inhibitory activity (IC_{50} = 2.5 μM) than substituted phenyl or heterocycles with hydroxy groups (**1g–m**). In addition, the compound with 4-hydroxyphenyl group on R_2 (**1c**) showed slightly better HIF-1α inhibitory activity (IC_{50} = 5 μM) than compounds with 2- or 3-hydroxyphenyl group (**1p** and **1q**, 8 and 8 μM, respectively). Docking study of

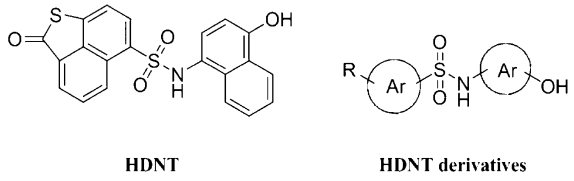

HDNT **HDNT derivatives**

Figure 1. Structures of HDNT and derivatives.

dx.doi.org/10.1021/jm500863j | J. Med. Chem. 2014, 57, 7990–7998

Table 1. HIF-1α Inhibitory Activity of HDNT Derivatives

compd	R_1	R_2	HIF-1α IC_{50} [a] (μM)
1a	4-methylphenyl	4-hydroxyphenyl	>20
1b	4-ethylphenyl	4-hydroxyphenyl	>20
1c	4-*tert*-butylphenyl	4-hydroxyphenyl	5
1d	4-*tert*-butylphenyl	4-hydroxynaphthalen-1-yl	>20
1e	4-*tert*-butylphenyl	8-hydroxyquinolin-5-yl	20
1f	4-biphenyl	4-hydroxyphenyl	2.5
1g	4-biphenyl	3-fluoro-4-hydroxyphenyl	>20
1h	4-biphenyl	3-chloro-4-hydroxyphenyl	>20
1i	4-biphenyl	3-carboxy-4-hydroxyphenyl	>20
1j	4-biphenyl	4-hydroxynaphthalen-1-yl	>20
1k	4-biphenyl	5-hydroxynaphthalen-1-yl	>20
1l	4-biphenyl	7-hydroxynaphthalen-1-yl	>20
1m	4-biphenyl	8-hydroxyquinolin-5-yl	20
1n	2-naphthyl	4-hydroxyphenyl	>20
1o	quinolin-8-yl	4-hydroxyphenyl	>20
1p	4-*tert*-butylphenyl	2-hydroxyphenyl	8
1q	4-*tert*-butylphenyl	3-hydroxyphenyl	8
2	4-biphenyl	potassium 4-phenolate	5
HDNT			20

[a]Experimental details are described in Experimental Section. Each value represents the mean from three independent experiments.

HDNT derivatives was performed using Discovery Studio program, and the results are shown in Supporting Information Figure S1. Hydrogen bond in the sulfonamide core and hydrophobic interaction between R_1 and Leu29 of UQCRB were observed, but hydrogen bond in hydroxyl group on R_2 was not observed. Among 17 HDNT derivatives, **1c**, **1e**, **1f**, and **1m** with good HIF-1α inhibitory activities (5, 20, 2.5, and 20 μM, respectively) were evaluated for the thermodynamic solubility (Table 2). **1f** with the best HIF-1α inhibitory activities showed low thermodynamic solubility (under 2.06 μg/mL in both PBS and H_2O solution). To improve the low solubility of **1f**, potassium salt formation was performed. Potassium salt compound **2** showed similar inhibitory activity with **1f** and improved solubility (Table 2). **1c**, **1f**, and **2** with good HIF-1α inhibitory activity have been selected for additional assays.

Competitive Binding Assays. In our previous reports, we demonstrated that the in vitro assay based on the competitive binding of biotin-labeled terpestacin to UQCRB can be successfully applied to the screening of novel small molecules binding with UQCRB.[14,21] To demonstrate the binding of **1c** and **1f** to UQCRB, we performed a surface plasmon resonance (BIAcore) based competitive binding assay using biotinylated terpestacin (BT). Controls of biotin and BT were sequentially immobilized onto the surface of a streptavidin-coated sensor chip, and the apparent binding affinities were calculated by subtracting resonance values of UQCRB binding to control biotin from those of UQCRB binding to BT. For competitive binding analyses, terpestacin, **1c**, and **1f** were each incubated with UQCRB protein and the complexes were subsequently injected into flow cells of the sensor chip. The competitive binding of terpestacin to UQCRB inhibited binding between BT and UQCRB, resulting in a significant decrease in resonance units (Figure 2). Similar to the preincubation of terpestacin, the binding efficiency of UQCRB to BT decreased by 40% by preincubation of either **1c** or **1f** with UQCRB, which confirmed that the two small molecules directly bind to UQCRB.

Regulation of Mitochondrial ROS-Induced Hypoxic Signal Transduction. UQCRB of mitochondrial complex III plays a crucial role in the oxygen sensing mechanism that regulates responses to hypoxia, and thus, the increase in UQCRB-mediated mitochondrial ROS generation during hypoxia triggers HIF-1α stabilization and consequently induces the expression of its target genes, such as VEGF.[15] To determine whether the binding of the new derivatives to UQCRB regulates the O_2 sensing function of UQCRB, we investigated the effects of **1c** and **1f** on the mitochondrial ROS-mediated hypoxic signal transmission procedure. HepG2 cells were pretreated with **1c** or **1f** for 30 min and then exposed to 1% O_2 for 10 min. Mitochondrial ROS levels were measured using the MitoSOX Red mitochondrial superoxide indicator. Compounds **1c** and **1f** suppressed the hypoxia-induced mitochondrial ROS generation in HepG2 cells in a dose-dependent manner (Figure 3A). Moreover, the compounds significantly inhibited HIF-1α accumulation and VEGF expression induced by hypoxia (Figures 3B,C). These results suggest that the binding of the new analogs to UQCRB modulates the O_2 sensing function of UQCRB. Notably, the derivatives did not affect cell viability at concentrations used in the present study, indicating that the effects of these compounds on cellular oxygen sensing do not result from off target toxicity (Supporting Information Figure S2).

In Vitro Angiogenesis Assay. Recently, our study investigating the role of UQCRB in angiogenesis revealed that UQCRB enhances VEGF receptor type 2 (VEGFR2) signaling by increasing the levels of mitochondrial ROS in ECs and terpestacin blocks mitochondrial ROS-mediated VEGFR2 signaling pathways, thereby inhibiting VEGF-induced angiogenesis of ECs.[20] Therefore, we evaluated the effects of the new mitochondrial UQCRB modulators on key angiogenic processes of ECs activated by VEGF. Serum-starved human umbilical vein endothelial cells (HUVECs) were stimulated by VEGF with or without **1c** or **1f** and in vitro angiogenesis assays were performed. The two compounds dose-dependently suppressed VEGF-induced invasion and tube formation of HUVECs (Figure 4). Trypan blue staining was performed in

Table 2. Thermodynamic Solubility of Active HDNT Derivatives

				thermodynamic solubility[a] (μg/mL)	
compd	R_1	R_2	HIF-1α IC_{50} (μM)	PBS	H_2O
1c	4-*tert*-butylphenyl	4-hydroxyphenyl	5	26.74	NT
1e	4-*tert*-butylphenyl	8-hydroxyquinolin-5-yl	20	12.84	NT
1f	4-biphenyl	4-hydroxyphenyl	2.5	<2.06	<2.06
1m	4-biphenyl	8-hydroxyquinolin-5-yl	20	7.26	NT
2	4-biphenyl	potassium 4-phenolate	5	108	>500

[a]Thermodynamic solubility was determined by HPLC. Values are the mean from three independent experiments. NT, not tested.

dx.doi.org/10.1021/jm500863j | J. Med. Chem. 2014, 57, 7990−7998

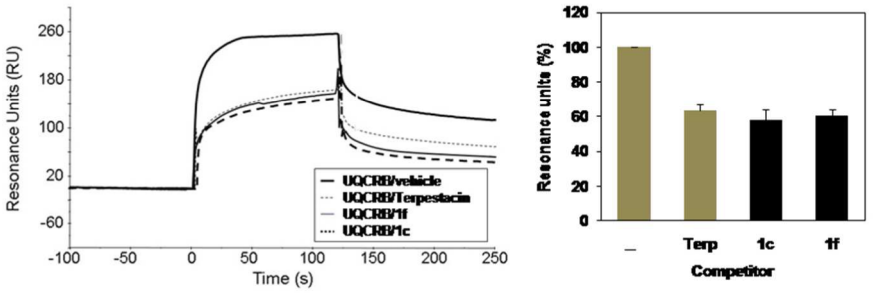

Figure 2. Effects of the competitors on the interaction between purified UQCRB protein and immobilized terpestacin (Terp) by SPR analysis.

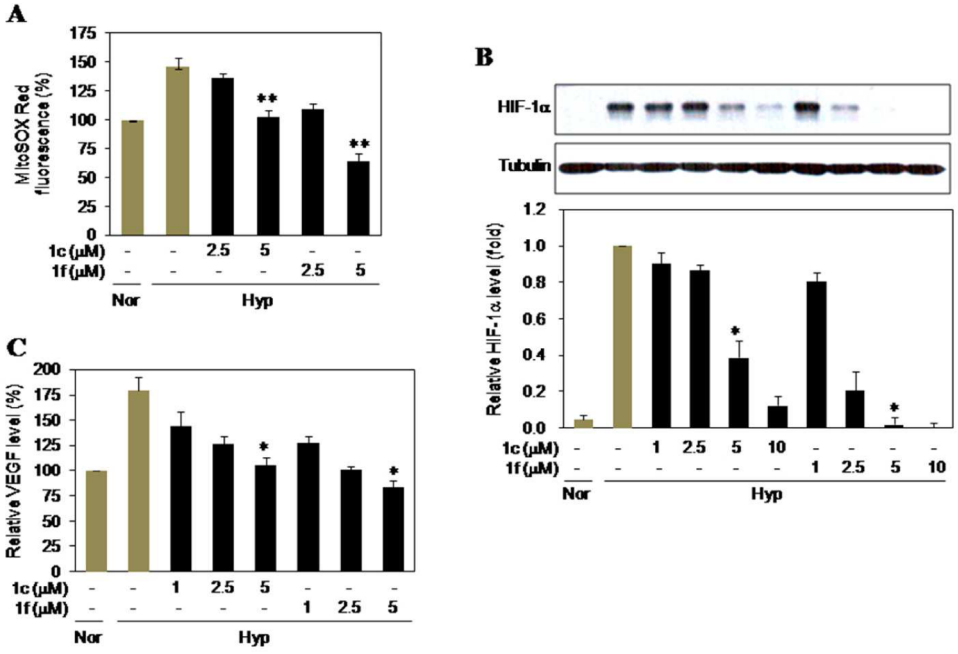

Figure 3. Regulation of mitochondrial ROS-mediated hypoxic signal transduction by new derivatives. (A) Effects of **1c** and **1f** on mitochondrial ROS generation. Mitochondrial ROS levels were determined by MitoSOX Red fluorescence. HepG2 cells were pretreated with compounds for 30 min and then exposed to 1% O_2 for 10 min: Nor, normoxia; Hyp, hypoxia. (**) $P < 0.01$ versus hypoxia control. (B) Effects of **1c** and **1f** on HIF-1α stability. HIF-1α protein levels were analyzed by Western blot analysis. HepG2 cells were pretreated with the compounds for 30 min and then exposed to 1% O_2 for 4 h. Western blot data were quantified using densitometry. (*) $P < 0.001$ versus hypoxia control. (C) Effect of **1c** and **1f** on VEGF expression. HepG2 cells were pretreated with compounds for 30 min and then exposed to 1% O_2 for 16 h. The concentration of VEGF protein in the culture supernatant was determined using an ELISA specific for VEGF. (*) $P < 0.001$ versus hypoxia control. Each value represents the mean ± SE from three independent experiments.

parallel with in vitro angiogenesis assays, and cytotoxicity was not observed at the indicated concentrations.

In Vivo Angiogenesis Assay. The antiangiogenic activity of the new UQCRB targeting small molecules was also validated in vivo by the chorioallantoic membrane (CAM) assay. Thermanox coverslips loaded with **1c** and **1f** were placed on the surface of CAM from growing chick embryos, and neovascularized zones were observed under the microscope. Retinoic acid (RA) was used as a positive control for antiangiogenic responses. As shown in Figure 5, RA inhibited angiogenesis by 67% (n = 9), whereas the control coverslips exhibited 23% (n = 13) inhibition. Compounds **1c** and **1f** effectively inhibited the neovascularization of CAM from chick embryos by 65% (n = 17) and 69% (n = 13), respectively, without inducing any rupture or toxicity to pre-existing vessels. These data demonstrate that the synthetic small molecules are a novel class of antiangiogenic agents targeting UQCRB.

Antitumor Activity in Vivo. Glioblastoma is one of the most aggressive angiogenic solid tumors and consequently highly resistant to chemotherapy.[22−24] Thus, we further determined the effects of the new UQCRB modulator **1f** on tumor growth and tumor angiogenesis in a glioblastoma mouse xenograft model. A pilot study was carried out, and **1f** administration notably inhibited the tumor growth despite its poor water solubility (Supporting Information Figure S3). In particular, a salt form of the compound (**2**) was synthesized to increase its aqueous solubility and biological activity was confirmed by its HIF-1α inhibition activity in HepG2 cells as well as antiproliferative effect in U87MG cells in vitro (Supporting Information Figures S4 and S5). Furthermore, we demonstrated that the bioactivity of **2** is not attributed to the nonspecific action as a highly active nucleophile by testing the phenoxide derivatives of other compounds (**1a** and **1c**; Supporting Information Table S1 and Figure S6). Next, BALB/c nude mice were inoculated with U87MG cells, and the mice were intraperitoneally administered with vehicle or **2**. As shown in Figures 6A,B, **2** led to a dramatic reduction in tumor growth without exhibiting significant body weight loss in mice.

dx.doi.org/10.1021/jm500863j | J. Med. Chem. 2014, 57, 7990−7998

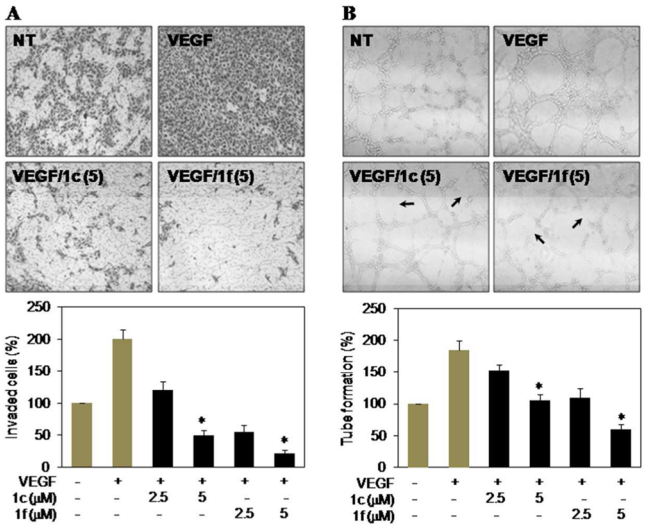

Figure 4. Effects of new derivatives on in vitro angiogenesis. Serum-starved HUVECs were stimulated with VEGF (30 ng/mL) in the presence or absence of **1c** and **1f**. (A) Inhibitory activity of the compounds on endothelial cell invasion. (B) Effects of the new analogs on the tube-forming ability of HUVECs. Arrows indicate inhibition of tube formation. The basal levels of invasiveness and capillary tube formation of HUVECs that were incubated in serum-free medium were normalized to 100%. (*) $P < 0.001$ versus VEGF control. Each value represents the mean ± SE from three independent experiments.

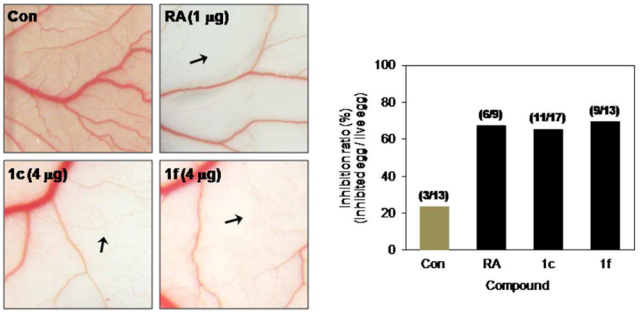

Figure 5. Effects of new compounds on the in vivo angiogenesis of CAM. Fertilized chick eggs were maintained in a humidified incubator at 37 °C. At the stage of a 4.5-day embryo, **1c**-, **1f**-, or RA-loaded Thermanox coverslips were applied to the CAM surface. Two days later, chorioallantois was observed under a microscope. When CAM that received treatment showed an avascular zone (arrows), the response was scored as positive. Calculations were based on the proportion of positive eggs relative to the total number of eggs tested.

Notably, **2** exhibited significantly increased antitumor activity compared to **lf**, indicating that its improved water solubility may contribute to the increase of clinical availability. We also evaluated the effects of **2** on tumor angiogenesis by measuring the tumor blood vessel density (using CD31 as an endothelial cell marker) and HIF-1α and VEGF expression levels. As shown in Figure 6C, **2** significantly decreased the tumor microvessel density and the expression of proangiogenic factors. These results imply that the new class of UQCRB modulators could be applied in new cancer therapeutics by blocking tumor angiogenesis.

CONCLUSION

Recently, we identified a natural antiangiogenic small molecule probe, terpestacin, that targets UQCRB of mitochondrial complex III, a protein that plays a critical role in tumor angiogenesis by mediating mitochondrial ROS generation in tumor cells and ECs.[14,20] The development of new small molecules targeting this protein may offer novel and effective cancer treatment strategies. By use of a reverse chemical genetics approach to discover new UQCRB modulators, a new synthetic small molecule HDNT was identified as a promising antiangiogenic agent targeting UQCRB.[21] In the present study, a SAR analysis was conducted to improve the pharmacological potential of HDNT.

In conclusion, this report describes the design, synthesis, and biological evaluation of a new series of HDNT derivatives with a sulfonylamide backbone. Notably, of the more potent derivatives, **1f** exhibited 8 times greater inhibitory potency than the parent small molecule HDNT in a cell-based assay that measured HIF-1α activity. The novel class of mitochondrial UQCRB modulators exhibited potent antiangiogenic activity without inducing cytotoxic effects both in vitro and in vivo by blocking mitochondrial ROS-mediated angiogenic signaling. Although the new compounds exhibited the in vitro binding efficiency to UQCRB to the same extent as terpestacin and HDNT, their antiangiogenic potential in vitro ($IC_{50} \leq 2.5$ μM) was 2−10 times stronger than that of the previously reported small molecules targeting UQCRB (terpestacin, $IC_{50} = 25$ μM; HDNT, $IC_{50} = 5$ μM).[13,21] These results indicate that the novel class of UQCRB modulators exhibit greater pharmacological properties compared to original compounds.

Furthermore, **1f**/**2** significantly suppressed tumor growth and tumor angiogenesis in a glioblastoma mouse xenograft model, suggesting that the new UQCRB modulator could be applied in new therapeutic approaches for human cancer treatment.

EXPERIMENTAL SECTION

Chemistry. All chemicals were obtained from commercial suppliers and used without further purification. All reactions were monitored by thin-layer chromatography (TLC) on precoated silica gel 60 F254 (mesh) (Merck, Mumbai, India), and spots were visualized under UV light (254 nm). Flash column chromatography was performed with silica (Merck EM9385, 230−400 mesh). ^{1}H and ^{13}C nuclear magnetic resonance (NMR, Varian Unity Inova) spectra were recorded at 400 and 100 MHz, respectively (Supporting Information Figure S7). Proton and carbon chemical shifts are expressed in ppm relative to the internal tetramethylsilane standard, and coupling constants (J) are expressed in hertz. Splitting patterns are presented as s, singlet; d, doublet; t, triplet; q, quartet; dd, double of doublets; m, multiplet; and br, broad. Liquid chromatography−mass spectrometry (LC−MS) spectra were obtained by using an electrospray ionization (ESI) probe using a Shimadzu LCMS2010 instrument with an Agilent C_{18} column (50 mm × 4.6 mm, 5 μm particle size). The mobile phase consisted of 0.1% formic acid in H_2O/0.1% formic acid in CH_3CN (1:9) over 10 min at a flow rate of 0.2 mL min^{-1}; the scan mode was ranged from 0 to 500 amu z^{-1}. In the positive mode, the detected ion peaks were $(M^+z)/z$, where M and z represent the molecular weight of the compound and charge (number of protons), respectively. High-resolution ESI-MS measurements were performed on a Micromass quadrupole-time of flight (Q-TOF) Acquity UPLC−mass system at Yonsei University in the positive mode. To determine the purity of the final compounds (**1a−q**), high performance liquid chromatography (HPLC) experiments were conducted using the Agilent analytical column Eclipse-XDB-C_{18} (150 mm × 4.6 mm, 5 μm) on Shimadzu HPLC 2010 instruments. All compounds tested in biological assays were ≥95% pure (Supporting Information Table S2).

General Procedure for the Preparation of Title Compounds 1a−q. Commercially available sulfonyl chloride (1 equiv) and amine (1.5 equiv) were dissolved in acetone (0.1 M), and then pyridine (3

dx.doi.org/10.1021/jm500863j | J. Med. Chem. 2014, 57, 7990−7998

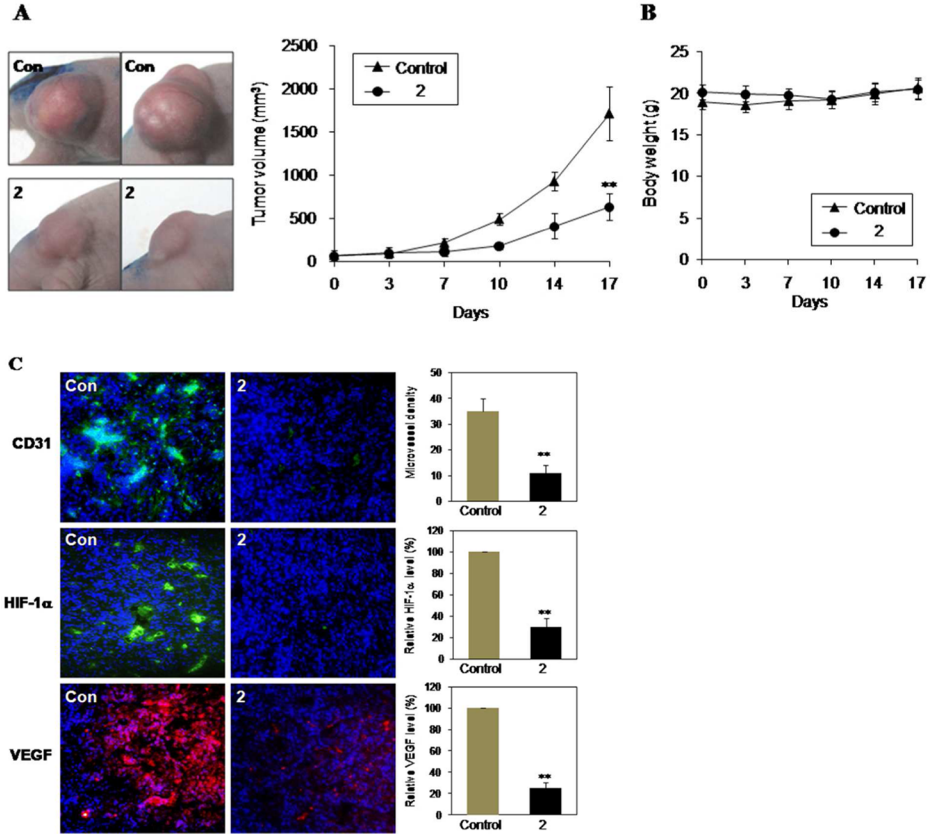

Figure 6. Antitumor and antiangiogenic activities of **2** in vivo. Mice bearing glioblastomas consisting of U87MG cells were treated with vehicle or **2** (20 mg/kg). (A) Tumor volumes of two groups (n = 8) after 17 days. (**) $P < 0.01$ versus vehicle control. (B) Body weight of mice. (C) Immunohistochemical staining for the detection of CD31, HIF-1α, and VEGF expression. The fluorescence images were originally obtained at 200× magnification. Quantification of the microvessel density was conducted by counting the number of positive structures in three random fields. The relative intensity of HIF-1α and VEGF expression was measured by the densitometric analysis of three random fields. (**) $P < 0.01$ versus vehicle control.

equiv) was added. The mixture was reacted using microwave reactor at 100 °C for 40 min. The reacted mixture was cooled and quenched with 10% HCl. The crude was extracted by ethyl acetate. Extracted organic layer was washed with brine, dried over anhydrous $MgSO_4$, filtered, and concentrated. The crude product was purified by flash column chromatography (ethyl acetate/hexane, 1:5 to 1:1).

***N*-(4-Hydroxyphenyl)-4-methylbenzenesulfonamide (1a).** ^{1}H NMR (400 MHz, DMSO-d_6) δ 7.67 (d, 2H, J = 8.4 Hz), 7.44 (d, 2H, J = 8.4 Hz), 6.60 (d, 2H, J = 8.8 Hz), 6.43 (d, 2H, J = 8.8 Hz), 2.41 (s, 3H); ^{13}C NMR (100 MHz, DMSO-d_6) δ 147.88, 145.31, 138.97, 131.70, 130.01, 128.24, 122.48, 113.89, 21.15; ESI (m/z) 262 (MH^-); HRMS (ESI) calcd for $C_{13}H_{13}NO_3S$ [MH^+] 264.0689, found 264.0675.

4-Ethyl-*N*-(4-hydroxyphenyl)benzenesulfonamide (1b). ^{1}H NMR (400 MHz, DMSO-d_6) δ 9.64 (s, 1H), 9.25 (s, 1H), 7.53 (d, 2H, J = 8.0 Hz), 7.31 (d, 2H, J = 8.4 Hz), 6.81 (d, 2H, J = 8.8 Hz), 6.56 (d, 2H, J = 8.8 Hz), 2.59 (q, 2H, J = 7.2 Hz), 1.11 (t, 3H, J = 7.6 Hz); ^{13}C NMR (100 MHz, DMSO-d_6) δ 155.1, 149.2, 137.4, 129.0, 128.7, 127.2, 124.2, 115.9, 28.3, 15.4; ESI (m/z) 276 (MH^-); HRMS (ESI) calcd for $C_{14}H_{15}NO_3S$ [MH^+] 278.0845, found 278.0823.

4-*tert*-Butyl-*N*-(4-hydroxyphenyl)benzenesulfonamide (1c). ^{1}H NMR (400 MHz, DMSO-d_6) δ 9.69 (s, 1H), 9.26 (s, 1H), 7.57 (d, 2H, J = 8.4 Hz), 7.50 (d, 2H, J = 8.4 Hz), 6.84 (d, 2H, J = 8.8 Hz), 6.57 (d, 2H, J = 8.8 Hz), 1.22 (s, 9H); ^{13}C NMR (100 MHz, DMSO-d_6) δ 155.51, 154.64, 136.93, 128.69, 126.57, 125.90, 123.50, 115.33, 34.84, 30.78; ESI (m/z) 304 (MH^-); HRMS (ESI) calcd for $C_{16}H_{19}NO_3S$ [MH^+] 306.1158, found 306.1133.

4-*tert*-Butyl-*N*-(4-hydroxynaphthalen-1-yl)benzenesulfonamide (1d). ^{1}H NMR (400 MHz, DMSO-d_6) δ 8.02 (d, 1H, J = 8.0 Hz), 7.74 (d, 2H, J = 8.4 Hz), 7.58 (d, 2H, J = 8.4 Hz), 7.53 (d, 1H, J = 7.6 Hz), 7.36−7.29 (m, 2H), 6.87 (d, 1H, J = 8.4 Hz), 6.50 (d, 1H, J = 8.0 Hz), 5.91 (s, 2H); ^{13}C NMR (100 MHz, DMSO-d_6) δ 155.53, 152.42, 137.35, 131.48, 126.61, 125.95, 125.76, 124.83, 124.62, 123.16, 122.05, 107.26, 34.79, 30.80; ESI (m/z) 354 (MH^-); HRMS (ESI) calcd for $C_{20}H_{21}NO_3S$ [MNa^+] 378.1134, found 378.1127.

4-*tert*-Butyl-*N*-(8-hydroxyquinolin-5-yl)benzenesulfonamide (1e). ^{1}H NMR (400 MHz, DMSO-d_6) δ 9.91 (s, 1H), 9.86 (s, 1H), 8.74 (dd, 1H, J_A = 4.0 Hz, J_B = 1.4 Hz), 8.11 (dd, 1H, J_A = 8.4 Hz, J_B = 1.4 Hz), 7.48−7.42 (m, 4H), 7.37−7.34 (m, 1H), 7.00 (d, 1H, J = 8.4 Hz), 6.93 (d, 1H, J = 8.0 Hz), 1.20 (s, 9H); ^{13}C NMR (100 MHz, DMSO-d_6) δ 156.2, 153.0, 148.5, 137.0, 127.0, 126.7, 126.3, 123.0, 121.9, 110.9, 35.2, 31.2; ESI (m/z) 357 (MH^+), 355 (MH^-); HRMS (ESI) calcd for $C_{19}H_{20}N_2O_3S$ [MNa^+] 379.1087, found 379.1088.

***N*-(4-Hydroxyphenyl)biphenyl-4-sulfonamide (1f).** ^{1}H NMR (400 MHz, DMSO-d_6) δ 9.76 (s, 1H), 9.29 (s, 1H), 7.79 (d, 2H, J = 8.4 Hz), 7.69 (t, 4H, J = 8.6 Hz), 7.47−7.37 (m, 3H), 6.85 (d, 2H, J = 8.8 Hz), 6.58 (d, 2H, J = 8.8 Hz); ^{13}C NMR (100 MHz, DMSO-d_6) δ 155.28, 144.35, 138.82, 138.74, 129.52, 128.94, 128.89, 127.80, 128.59, 127.45, 124.39, 115.89; ESI (m/z) 324 (MH^-); HRMS (ESI) calcd for $C_{18}H_{15}NO_3S$ [MH^-] 324.0700, found 324.0705.

***N*-(3-Fluoro-4-hydroxyphenyl)biphenyl-4-sulfonamide (1g).** ^{1}H NMR (400 MHz, DMSO-d_6) δ 10.03 (s, 1H), 9.72 (s, 1H), 7.81 (d, 2H, J = 8.8 Hz), 7.74 (d, 2H, J = 8.4 Hz), 7.67 (d, 2H, J = 7.2 Hz), 7.47−7.38 (m, 3H), 6.85 (dd, 1H, J_A = 6.4 Hz, J_B = 2.4 Hz), 6.78 (t, 1H, J = 9.2 Hz), 6.69 (dd, 1H, J_A = 4.4 Hz, J_B = 1.6 Hz); ^{13}C NMR (100 MHz, DMSO-d_6) δ 152.05, 149.65, 144.61, 142.60, 142.48, 138.67, 138.45, 129.52, 127.79, 127.46, 118.50, 118.34, 110.68, 110.47; ESI (m/z) 342 (MH^-); HRMS (ESI) calcd for $C_{18}H_{14}FNO_3S$ [MH^+] 344.0751, found 344.0733.

dx.doi.org/10.1021/jm500863j | J. Med. Chem. 2014, 57, 7990−7998

***N*-(3-Chloro-4-hydroxyphenyl)biphenyl-4-sulfonamide (1h).** ^{1}H NMR (400 MHz, DMSO-d_6) δ 10.07 (s, 1H), 10.03 (s, 1H), 7.81 (d, 2H, J = 8.4 Hz), 7.74 (d, 2H, J = 8.4 Hz), 7.66 (d, 2H, J = 7.2 Hz), 7.44 (t, 2H, J = 7.4 Hz), 7.39 (d, 1H, J = 7.2 Hz), 7.02 (d, 1H, J = 2.4 Hz), 6.88 (dd, 1H, J_A = 4.4 Hz, J_B = 2.4 Hz), 6.82(d, 1H, J = 8.8 Hz); ^{13}C NMR (100 MHz, DMSO-d_6) δ 150.93, 144.63, 138.66, 138.42, 129.82, 129.52, 128.99, 127.80, 127.74, 127.45, 123.80, 122.37, 119.94, 117.30; ESI (m/z) 358 (MH^-); HRMS (ESI) calcd for $C_{18}H_{14}ClNO_3S$ [MH^+] 360.0456, found 360.0451.

5-(Biphenyl-4-ylsulfonamido)-2-hydroxybenzoic Acid (1i). ^{1}H NMR (400 MHz, DMSO-d_6) δ 10.11 (s, 1H), 7.80 (d, 2H, J = 8.4 Hz), 7.72 (d, 2H, J = 8.4 Hz), 7.66 (d, 2H, J = 7.6 Hz), 7.49 (d, 1H, J = 2.8 Hz), 7.44 (t, 2H, J = 7.4 Hz), 7.38 (d, 1H, J = 7.6 Hz), 7.23 (dd, 1H, J_A = 4.5 Hz, J_B = 2.6 Hz), 6.84 (d, 1H, J = 8.8 Hz); ^{13}C NMR (100 MHz, DMSO-d_6) δ 171.58, 158.75, 144.62, 138.64, 138.38, 130.43, 129.52, 129.19, 128.99, 127.79, 127.74, 127.45, 123.79, 118.35, 113.44; ESI (m/z) 368 (MH^-); HRMS (ESI) calcd for $C_{19}H_{15}NO_5S$ [MH^-] 368.0598, found 368.0596.

***N*-(4-Hydroxynaphthalen-1-yl)biphenyl-4-sulfonamide (1j).** ^{1}H NMR (400 MHz, DMSO-d_6) δ 8.09 (d, 1H, J = 8.4 Hz), 7.94 (q, 4H, J = 8.4 Hz), 7.75−7.70 (m, 3H), 7.54−7.39 (m, 5H), 6.94 (d, 1H, J = 8.4 Hz), 6.56 (d, 1H, J = 8.0 Hz), 5.98 (s, 2H); ^{13}C NMR (100 MHz, DMSO-d_6) δ 146.42, 144.92, 138.33, 135.07, 134.08, 129.63, 129.38, 129.31, 128.11, 127.61, 126.91, 124.85, 123.14, 121.48, 120.18, 105.90; ESI (m/z) 374 (MH^-); HRMS (ESI) calcd for $C_{22}H_{17}NO_3S$ [MH^+] 376.1002, found 376.1002.

***N*-(5-Hydroxynaphthalen-1-yl)biphenyl-4-sulfonamide (1k).** ^{1}H NMR (400 MHz, DMSO-d_6) δ 8.03 (d, 1H, J = 8.4 Hz), 7.97 (d, 2H, J = 8.4 Hz), 7.90 (d, 2H, J = 8.8 Hz), 7.70 (d, 2H, J = 7.2 Hz), 7.50−7.43 (m, 3H), 7.30 (t, 1H, J = 8.0 Hz), 7.18−7.14 (m, 2H), 7.01 (d, 1H, J = 8.4 Hz), 6.66 (d, 1H, J = 7.6 Hz), 5.88 (s, 2H); ^{13}C NMR (100 MHz, DMSO-d_6) δ 146.59, 145.59, 145.49, 138.27, 134.09, 129.64, 129.43, 129.22, 128.35, 128.23, 128.21, 127.64, 124.39, 123.15, 122.43, 118.32, 108.65, 108.53; ESI (m/z) 376 (MH^+), 374 (MH^-); HRMS (ESI) calcd for $C_{22}H_{17}NO_3S$ [MH^+] 376.1001, found 376.1002.

***N*-(7-Hydroxynaphthalen-1-yl)biphenyl-4-sulfonamide (1l).** ^{1}H NMR (400 MHz, DMSO-d_6) δ 8.04 (d, 1H, J = 9.2 Hz), 7.92 (s, 4H), 7.72 (d, 2H, J = 7.6 Hz), 7.50−7.43 (m, 4H), 7.19 (t, 1H, J = 7.8 Hz), 7.00−6.95 (m, 2H), 6.65 (d, 1H, J = 7.8 Hz), 5.81 (s, 2H); ^{13}C NMR (100 MHz, DMSO-d_6) δ 146.98, 146.55, 145.46, 138.23, 134.95, 133.51, 129.65, 129.45, 129.38, 128.74, 128.19, 127.64, 125.35, 121.46, 119.88, 118.40, 115.57, 108.48; ESI (m/z) 376 (MH^+), 374 (MH^-); HRMS (ESI) calcd for $C_{22}H_{17}NO_3S$ [MH^+] 376.1002, found 376.1004.

***N*-(8-Hydroxyquinolin-5-yl)biphenyl-4-sulfonamide (1m).** ^{1}H NMR (400 MHz, DMSO-d_6) δ 8.62 (d, 1H, J = 4.0 Hz), 8.47 (d, 1H, J = 8.4 Hz), 7.89 (d, 2H, J = 8.4 Hz), 7.81 (d, 2H, J = 8.4 Hz), 7.67 (d, 2H, J = 7.2 Hz), 7.49−7.41 (m, 3H), 7.33−7.30 (m, 1H), 7.21 (d, 1H, J = 8.4 Hz), 6.58 (d, 1H, J = 8.8 Hz), 6.17 (s, 2H); ^{13}C NMR (100 MHz, DMSO-d_6) δ 150.60, 146.02, 145.46, 141.83, 138.55, 134.69, 134.60, 131.55, 129.59, 129.47, 129.24, 127.60, 127.56, 124.00, 119.87, 118.18, 105.93; ESI (m/z) 377 (MH^+), 375 (MH^-); HRMS (ESI) calcd for $C_{21}H_{16}N_2O_3S$ [MH^+] 377.0954, found 377.0954.

***N*-(4-Hydroxyphenyl)naphthalene-2-sulfonamide (1n).** ^{1}H NMR (400 MHz, DMSO-d_6) δ 8.46 (s, 1H), 8.18−8.15 (m, 2H), 8.07 (d, 1H, J = 8.4 Hz), 7.80−7.73 (m, 2H), 7.67 (t, 1H, J = 7.2 Hz), 6.58 (d, 2H, J = 8.8 Hz), 6.35 (d, 2H, J = 9.2 Hz), 5.15 (s, 2H); ^{13}C NMR (100 MHz, DMSO-d_6) δ 147.94, 138.95, 134.93, 131.43, 129.81, 129.57, 127.97, 122.71, 122.49, 113.89; ESI (m/z) 298 (MH^-); HRMS (ESI) calcd for $C_{16}H_{13}NO_3S$ [MH^+] 300.0689, found 300.0685.

***N*-(4-Hydroxyphenyl)quinoline-8-sulfonamide (1o).** ^{1}H NMR (400 MHz, DMSO-d_6) δ 9.12 (d, 1H, J = 4.4 Hz), 8.50 (d, 1H, J = 8.0 Hz), 8.22−8.17 (m, 2H), 7.72−7.69 (m, 1H), 7.63 (t, 1H, J = 7.8 Hz), 6.70 (d, 2H, J = 8.4 Hz), 6.41 (d, 2H, J = 8.4 Hz); ^{13}C NMR (100 MHz, DMSO-d_6) δ 155.06, 151.81, 143.14, 137.44, 135.71, 134.34, 132.21, 128.96, 126.05, 124.00, 123.03, 115.66, 68.68, 27.84, 22.16; ESI (m/z) 299 (MH^-); HRMS (ESI) calcd for $C_{15}H_{12}N_2O_3S$ [MH^+] 301.0641, found 301.0643.

4-*tert*-Butyl-*N*-(2-hydroxyphenyl)benzenesulfonamide (1p). ^{1}H NMR (400 MHz, DMSO-d_6) δ 9.36 (s, 2H), 7.68 (d, 2H, J = 8.4 Hz), 7.50 (d, 2H, J = 8.4 Hz), 7.12 (d, 1H, J = 8.0 Hz), 6.88 (t, 1H, J = 7.8 Hz), 6.71 (d, 1H, J = 8.0 Hz), 6.65 (t, 1H, J = 7.6 Hz), 1.23 (s, 1H); ^{13}C NMR (100 MHz, DMSO-d_6) δ 155.87, 150.17, 138.38, 126.99, 126.19, 126.16, 124.80, 124.04, 119.36, 115.93, 35.24, 31.21; ESI (m/z) 306 (MH^+), 304 (MH^-); HRMS (ESI) calcd for $C_{16}H_{19}NO_3S$ [MH^-] 304.1013, found 304.1008.

4-*tert*-Butyl-*N*-(3-hydroxyphenyl)benzenesulfonamide (1q). ^{1}H NMR (400 MHz, DMSO-d_6) δ 10.13 (s, 1H), 9.41 (s, 1H), 7.67 (d, 2H, J = 8.4 Hz), 7.54 (d, 2H, J = 8.8 Hz), 6.94 (t, 1H, J = 7.8 Hz), 6.57 (t, 1H, J = 2.0 Hz), 6.50 (d, 1H, J = 8.0 Hz), 6.35 (dd, 1H, J_A = 4.0 Hz, J_B = 2.0 Hz), 1.23 (s, 9H); ^{13}C NMR (100 MHz, DMSO-d_6) δ 158.26, 156.18, 139.36, 137.42, 130.25, 126.92, 126.52, 111.22, 110.33, 106.72, 35.29, 31.16; ESI (m/z) 306 (MH^+), 304 (MH^-); HRMS (ESI) calcd for $C_{16}H_{19}NO_3S$ [MH^-] 304.1013, found 304.1006.

General Procedure for the Preparation of Title Compound 2. To a solution of **1f** in EtOH, 1 M solution of KOH in EtOH (1.1 equiv) was added at 0 °C. The reaction mixture was warmed to room temperature and filtered after salt formed. The precipitate was washed by EtOH three times and dried in vacuo.

Potassium 4-(Biphenyl-4-ylsulfonamido)phenolate (2). ^{1}H NMR (400 MHz, DMSO-d_6) δ 7.77−7.68 (m, 6H), 7.48 (t, 2H, J = 7.6 Hz), 7.40 (t, 1H, J = 7.2 Hz), 6.81 (d, 2H, J = 8.8 Hz), 6.55 (d, 2H, J = 8.8 Hz); ^{13}C NMR (100 MHz, DMSO-d_6) δ 155.29, 144.36, 138.81, 138.74, 129.52, 127.81, 127.59, 127.44, 124.40, 116.00; ESI (m/z) 324 (M^-).

HIF-1α Stability Analysis. HepG2 cells were pretreated with the indicated concentrations of the synthetic derivatives for 30 min and then exposed to 1% O_2 for 4 h. HIF-1α and tubulin protein levels were analyzed by Western blot analysis and quantified using densitometry.

Competitive Binding Assays by SPR. Biotin and biotinylated terpestacin were sequentially immobilized onto the surface of a streptavidin-coated sensor chip. Competitors (25 μM) were incubated with purified UQCRB protein (25 μM) in pH 7.4 running buffer (10 mM HEPES, 150 mM NaCl, and 3 mM EDTA), and then UQCRB−competitor complexes were injected onto the sensor chip at a flow rate of 30 μL/min. The surface of the sensor chip was regenerated by injecting 5 μL of regeneration buffer (50 mM NaOH). Molecular interaction analysis was performed using the BIAcore 2000 system (BIAcoreAB), and apparent binding affinities were calculated by subtracting resonance values of UQCRB binding to control biotin from those of UQCRB binding to biotinylated terpestacin.

Measurement of Mitochondrial ROS. Mitochondrial ROS levels were measured using a MitoSOX Red mitochondrial superoxide indicator (Invitrogen). Once in the mitochondria, the MitoSOX Red reagents oxidized by superoxide emit red fluorescence. HepG2 cells were pretreated with indicated concentrations of synthetic derivatives for 30 min and then exposed to 1% O_2 for 10 min. After incubation with MitoSOX Red (5 μM) for 10 min, cells were lysed and centrifuged to remove debris. The fluorescence in the protein-normalized supernatant was determined using a FL600 microplate fluorescence reader (Bio-Tek) at the excitation and emission wavelengths of 510 and 580 nm, respectively.

In Vitro Angiogenesis Assays. The invasiveness of HUVECs was examined using a Transwell chamber system with 8.0 μm pore-sized polycarbonate filter inserts (Corning Costar, Acton, MA, USA) as previously described.[25,26] The total number of invaded cells was counted using an optical microscope at 100× magnification. The tube formation assay was performed using HUVECs grown on Matrigel (BD Biosciences, San Jose, CA, USA) as previously described.[25] Tube formation was quantified by counting the number of connected cells in randomly selected fields at 100× magnification and dividing that number by the total number of cells in the same field.

CAM Assay. Fertilized chick eggs were maintained in a humidified incubator at 37 °C for 3 days. Approximately 2 mL of egg albumin was removed with a hypodermic needle allowing the CAM and yolk sac to drop away from the shell membrane. On day 3.5 the shell was punched

out and removed, and the shell membrane was peeled away. When the chick embryos were 4.5 days old, Thermanox coverslips (NUNC, Rochester, NY, USA) containing the synthetic compounds were air-dried and then applied to the CAM surface. Two days later, 2 mL of 10% fat emulsion (Greencross Co., Yongin, South Korea) was injected into the chorioallantois, and the CAM was observed under a microscope. Because retinoic acid (RA) is a known antiangiogenic compound, RA was used as a positive control for antiangiogenic responses. The response was scored as positive when CAM treated with the sample showed an avascular zone similar to that of RA-treated CAM with very few vessels compared to that of the control coverslip. The response was calculated as the percentage of positive eggs relative to the total number of eggs tested.

In Vivo Mouse Tumor Xenograft Assay. All mice were housed in the specific pathogen-free (SPF) facility of the Laboratory Animal Research Center (LARC) in Yonsei University, which is operated in accordance with the Institutional Animal Care and Use Committee (IACUC) and international guidelines on the ethical use of animals. U87MG glioblastoma cells (5×10^6) suspended in 200 μL of PBS/Matrigel (1:1) were subcutaneously implanted into the dorsal flank of athymic nude mice (4 week-old female Balb C nu/nu, OrientBio). Once the tumors became palpable (50–100 mm^3), mice were randomly divided into two groups (n = 8, per group) and intraperitoneally treated with vehicle or **2** at a dosage of 20 mg/kg every other day. The tumor volume and body weight of the mice were measured twice a week using the following formula: $^{\pi}/_{6} \times$ length $\times$ width $\times$ height. On day 18, the tumor-bearing mice were sacrificed, and the tumors were excised, formalin-fixed, and paraffin-embedded for immunohistochemical analysis.

Immunohistochemistry. Four-micrometer paraffin sections were incubated with anti-CD31 (BD Biosciences), anti-HIF-1α (Novus, Littleton, CO, USA), and anti-VEGF (Santa Cruz, CA, USA) antibodies overnight at 4 °C. After rinsing, the sections were incubated with FITC- or Alexa-conjugated secondary antibodies (Invitrogen) for 45 min at room temperature and then counterstained with DAPI (Vector Laboratories, Cambridgeshire, U.K.). The images were obtained using an IX71 fluorescence microscope (Olympus) equippeda DP70 camera at 200× magnification. Quantification of microvessel density was conducted by counting the number of positive structures in three random fields. HIF-1α and VEGF levels were quantified by densitometric analysis of three random fields.

Statistical Analysis. Results are expressed as the mean ± standard error (SE). Student's t-test was used to determine the statistical significance between the control and test groups. A p value of <0.05 was considered to be statistically significant.

■ ASSOCIATED CONTENT

Ⓢ Supporting Information

Analytical data (HPLC analysis and NMR spectra) for all synthetic compounds, docking study, and biological assays. This material is available free of charge via the Internet at http://pubs.acs.org.

■ AUTHOR INFORMATION

Corresponding Author

*Telephone: +82-2-2123-5883. Fax: +82-2-362-7265. E-mail: kwonhj@yonsei.ac.kr.

Author Contributions

‖H.J.J. and M.C. contributed equally to this work.

Notes

The authors declare no competing financial interest.

■ ACKNOWLEDGMENTS

We are grateful to Dr. Chulho Lee for his help with the SAR study. This study was partly supported by grants from the National Research Foundation of Korea funded by the Korean Government (Grants 2009-0092964, 2010-0017984, and 2012M3A9D1054520), the Translational Research Center for Protein Function Control, KRF (Grant 2009-0083522), the Next-Generation BioGreen 21 Program (Grant PJ0079772012), Rural Development Administration, National R&D Program, Ministry of Health &Welfare (Grant 0620360-1), and the Brain Korea 21 Plus Project, Republic of Korea.

■ ABBREVIATIONS USED

UQCRB, ubiquinol–cytochrome c reductase binding protein; ROS, reactive oxygen species; HDNT, 6-((1-hydroxynaphthalen-4-ylamino)dioxysulfone)-2*H*-naphtho[1,8-*bc*]thiophen-2-one; HIF-1α, hypoxia inducible factor 1α; VEGF, vascular endothelial growth factor; EC, endothelial cell; SPR, surface plasmon resonance; BT, biotinylated terpestacin; VEGFR2, vascular endothelial growth factor receptor type 2; HUVEC, human umbilical vein endothelial cell; CAM, chorioallantoic membrane; RA, retinoic acid

■ REFERENCES

(1) Folkman, J. Angiogenesis-dependent diseases. *Semin. Oncol.* **2001**, *28*, 536–542.

(2) Carmeliet, P.; Jain, R. K. Angiogenesis in cancer and other diseases. *Nature* **2000**, *407*, 249–257.

(3) André, T.; Chastre, E.; Kotelevets, L.; Vaillant, J. C.; Louvet, C.; Balosso, J.; Le Gall, E.; Prévot, S.; Gespach, C. Tumoral angiogenesis: physiopathology, prognostic value and therapeutical prospects. *Rev. Med. Intern.* **1998**, *19*, 904–913.

(4) Battegay, E. J. Angiogenesis: mechanistic insights, neovascular disease, and therapeutic prospects. *J. Mol. Med.* **1995**, *73*, 333–346.

(5) Folkman, J. Fundamental concepts of the angiogenic process. *Curr. Mol. Med.* **2003**, *3*, 643–651.

(6) Olsson, A. K.; Dimberg, A.; Kreuger, J.; Claesson-Welsh, L. VEGF receptor signalling—in control of vascular function. *Nat. Rev. Mol. Cell Biol.* **2006**, *7*, 359–371.

(7) Nguyen, M.; Arkell, J.; Jackson, C. J. Human endothelial gelatinases and angiogenesis. *Int. J. Biochem. Cell Biol.* **2001**, *33*, 960–970.

(8) Kruger, E. A.; Figg, W. D. TNP-470: an angiogenesis inhibitor in clinical development for cancer. *Expert Opin. Invest. Drugs* **2000**, *9*, 1383–1396.

(9) Gryder, B. E.; Sodji, Q. H.; Oyelere, A. K. Targeted cancer therapy: giving histone deacetylase inhibitors all they need to succeed. *Future Med. Chem.* **2012**, *4*, 505–524.

(10) Verheul, H. M.; Pinedo, H. M. Possible molecular mechanisms involved in the toxicity of angiogenesis inhibition. *Nat. Rev. Cancer* **2007**, *7*, 475–485.

(11) Cook, K. M.; Figg, W. D. Angiogenesis inhibitors: current strategies and future prospec. *Ca—Cancer J. Clin.* **2010**, *60*, 222–243.

(12) Miller, K.; Wang, M.; Gralow, J.; Dickler, M.; Cobleigh, M.; Perez, E. A.; Shenkier, T.; Cella, D.; Davidson, N. E. Paclitaxel plus bevacizumab versus paclitaxel alone for metastatic breast cancer. *N. Engl. J. Med.* **2007**, *357*, 2666–2676.

(13) Jung, H. J.; Lee, H. B.; Kim, C. J.; Rho, J. R.; Shin, J.; Kwon, H. J. Anti-angiogenic activity of terpestacin, a bicyclo sesterterpene from *Embellisia chlamydospora*. *J. Antibiot. (Tokyo)* **2003**, *56*, 492–496.

(14) Jung, H. J.; Shim, J. S.; Lee, J.; Song, Y. M.; Park, K. C.; Choi, S. H.; Kim, N. D.; Yoon, J. H.; Mungai, P. T.; Schumacker, P. T.; Kwon, H. J. Terpestacin inhibits tumor angiogenesis by targeting UQCRB of mitochondrial complex III and suppressing hypoxia-induced reactive oxygen species production and cellular oxygen sensing. *J. Biol. Chem.* **2010**, *285*, 11584–11595.

(15) Cho, Y. S.; Jung, H. J.; Seok, S. H.; Payumo, A. Y.; Chen, J. K.; Kwon, H. J. Functional inhibition of UQCRB suppresses angiogenesis in zebrafish. *Biochem. Biophys. Res. Commun.* **2013**, *433*, 396–400.

(16) Wang, G. L.; Jiang, B. H.; Rue, E. A.; Semenza, G. L. Hypoxia-inducible factor 1 is a basic-helix-loop-helix-PAS heterodimer regulated

by cellular O_2 tension. *Proc. Natl. Acad. Sci. U.S.A.* **1995**, *92*, 5510−5514.
(17) Chandel, N. S.; Maltepe, E.; Goldwasser, E.; Mathieu, C. E.; Simon, M. C.; Schumacker, P. T. Mitochondrial reactive oxygen species trigger hypoxia-induced transcription. *Proc. Natl. Acad. Sci. U.S.A.* **1998**, *95*, 11715−11720.
(18) Brunelle, J. K.; Bell, E. L.; Quesada, N. M.; Vercauteren, K.; Tiranti, V.; Zeviani, M.; Scarpulla, R. C.; Chandel, N. S. Oxygen sensing requires mitochondrial ROS but not oxidative phosphorylation. *Cell Metab.* **2005**, *1*, 409−414.
(19) Guzy, R. D.; Hoyos, B.; Robin, E.; Chen, H.; Liu, L.; Mansfield, K. D.; Simon, M. C.; Hammerling, U.; Schumacker, P. T. Mitochondrial complex III is required for hypoxia-induced ROS production and cellular oxygen sensing. *Cell Metab.* **2005**, *1*, 401−408.
(20) Jung, H. J.; Kim, Y.; Chang, J.; Kang, S. W.; Kim, J. H.; Kwon, H. J. Mitochondrial UQCRB regulates VEGFR2 signaling in endothelial cells. *J. Mol. Med. (Berlin)* **2013**, *91*, 1117−1128.
(21) Jung, H. J.; Kim, K. H.; Kim, N. D.; Han, G.; Kwon, H. J. Identification of a novel small molecule targeting UQCRB of mitochondrial complex III and its anti-angiogenic activity. *Bioorg. Med. Chem. Lett.* **2011**, *21*, 1052−1056.
(22) Machein, M. R.; Plate, K. H. VEGF in brain tumors. *J. Neuro-Oncol.* **2000**, *50*, 109−120.
(23) Bao, S.; Wu, Q.; Sathornsumetee, S.; Hao, Y.; Li, Z.; Hjelmeland, A. B.; Shi, Q.; McLendon, R. E.; Bigner, D. D.; Rich, J. N. Stem cell-like glioma cells promote tumor angiogenesis through vascular endothelial growth factor. *Cancer Res.* **2006**, *66*, 7843−7848.
(24) Fischer, I.; Gagner, J. P.; Law, M.; Newcomb, E. W.; Zagzag, D. Angiogenesis in gliomas: biology and molecular pathophysiology. *Brain Pathol.* **2005**, *15*, 297−310.
(25) Jeon, K. S.; Na, H. J.; Kim, Y. M.; Kwon, H. J. Antiangiogenic activity of 4-*O*-methylgallic acid from *Canavalia gladiata*, a dietary legume. *Biochem. Biophys. Res. Commun.* **2005**, *330*, 1268−1274.
(26) Cheong, H. J.; Lee, K. S.; Woo, I. S.; Won, J. H.; Byun, J. H. Up-regulation of the DR5 expression by proteasome inhibitor MG132 augments TRAIL-induced apoptosis in soft tissue sarcoma cell lines. *Cancer Res. Treat.* **2011**, *43*, 124−130.